Clay Minerals (2021), **56**, 222–228
doi:10.1180/clm.2021.36

CAMBRIDGE UNIVERSITY PRESS

Article

Sepiolite as an efficient adsorbent for ethylene gas

Burcu Erdoğan[1]* and Fahri Esenli[2]

[1]Eskisehir Technical University, Faculty of Science, Department of Physics, 26470, Eskisehir, Turkey and [2]Istanbul Technical University, Faculty of Mines, Geological Engineering Department, Istanbul, Turkey

Abstract

The ability of Na^+-, Li^+-, K^+-, Ca^{2+}- and Mg^{2+}-exchanged sepiolites and acid-activated sepiolites to remove ethylene from storage environments was examined. The sepiolite from Sivrihisar deposit, Turkey, was treated with 1.0 M $NaNO_3$, $LiNO_3$, KNO_3, $Ca(NO_3)_2$, $Mg(NO_3)_2$, HNO_3 and H_2SO_4 solutions at 90°C for 4 h. The mineralogical, chemical and textural properties of the materials were examined using X-ray diffraction, X-ray fluorescence, cation-exchange capacity and nitrogen gas adsorption analyses. The main mineral phase present in the materials was sepiolite, with minor dolomite, and traces of quartz and feldspar minerals and amorphous matter. Adsorption isotherms of ethylene at 273 K were measured on sepiolite samples over a pressure range of 0–100 kPa. As a result of partial blockage of the sepiolite channels, the ethylene adsorption capacity on cation-exchanged sepiolite forms (0.376–0.907 mmol g^{-1}) was less than that of acid-activated sepiolite forms (1.279 and 1.308 mmol g^{-1}). The ethylene adsorption capacities of the sepiolite samples were compared with those of other clay-based materials (0.167–1.817 mmol g^{-1}) reported in previous studies of ethylene removal.

Keywords: adsorption, BET, ethylene, sepiolite, XRD

(Received 21 August 2021; revised 26 December 2021; Accepted Manuscript online: 5 January 2022; Associate Editor: Miroslav Pospíšil)

Sepiolite is a trioctahedral hydrated magnesium silicate with a chain structure, fibrous morphology and theoretical unit cell formula of $Mg_8[Si_{12}O_{30}](OH)_4(H_2O)_4.nH_2O$ (n = 6–8) (Galán, 1996; Murray, 2007; Suarez & Garcia-Romero, 2011). The structure of sepiolite consists of ribbons with a 2:1 phyllosilicate structure. These ribbons run parallel to the *x*-axis and have an average width along the *y*-axis of three linked pyroxene-like single chains. They contain continuous tetrahedral sheets that are inverted *via* basal oxygens, thus forming a discontinuous octahedral sheet (Jones & Galán, 1988; Galán, 1996; Murray, 2007; Brigatti *et al.*, 2006). These inverted tetrahedra occur regularly, forming channels (3.7 Å × 10.6 Å) (Galán, 1996). In addition to the exchangeable cations, these channels may also contain water that is coordinated to the octahedral cations and zeolitic water, which is loosely bonded in the channels (Galán 1996). The palygorskite–sepiolite group of clay minerals has a wide range of industrial applications because the fibrous crystal structure, large specific surface area and active silanol groups provide excellent adsorption properties. The cation-exchange capacity (CEC) of sepiolite (and palygorskite) ranges from 4 to 40 cmol(+) kg^{-1}, which may increase depending on impurities (Gal án, 1996).

Mild acid treatment is used widely to increase the specific surface area and to improve the purity and the adsorption capacity of sepiolite for gases and heavy metal ions. In this process, a certain proportion of the structural Mg^{2+} ions and metal exchange cations are removed and mineralogical impurities such as calcite and dolomite are eliminated. Thus, a partially dissolved material with increased specific surface area, porosity and surface acidity forms (Komadel, 2003). With more intense acid treatment the octahedral sheets dissolve, yielding free amorphous silica gel. The silica gel has variable textural characteristics depending on the nature of the raw material, the acid concentration, the reaction time and the reaction temperature (Rodriguez-Reinoso *et al.*, 1981; Vicente Rodriguez *et al.*, 1994; Myriam *et al.*, 1998; Komadel & Madejová, 2006).

Ethylene is a natural plant-growth regulator and it is highly effective in the development of leaves, flowers and fruits (Reid, 1995; Youngjan, 2012; Iqbal *et al.*, 2017). Accumulation of ethylene may be detrimental to fruit quality (Youngjan, 2012; Iqbal *et al.*, 2017). Therefore, the ethylene concentration must be controlled and excess ethylene must be removed from storage environments in order to prolong the storability and shelf-life of harvests. Despite its widespread use in ethylene retention, commercial $KMnO_4$ is an expensive contaminant material.

In addition to the abundance of sepiolite reserves in the Sivrihisar region, the large specific surface area of this sepiolite due to its molecular-sized channels is the main reason for choosing this low-cost material for this study. Previous studies of ethylene adsorption by clay-based materials (Choundary *et al.*, 2002; Park *et al.*, 2002, 2004; Cho *et al.*, 2005; Lee *et al.*, 2005; Saini *et al.*, 2011; Youngjan, 2012; Gwak *et al.*, 2017; Alvarez-Hernandez *et al.*, 2018; Srithammaraj *et al.*, 2018; Gaikwad *et al.*, 2019), acid-treated sepiolite, kaolinite and bentonite (Erdoğan Alver & Sakızcı, 2012; Erdoğan Alver *et al.*, 2016) and Ag^+-, K^+-, Li^+-, Mg^{2+}-, Cu^{2+}- and Fe^{3+}-exchanged bentonites (Erdoğan Alver & Günal, 2016; Erdoğan Alver, 2017) did not examine ethylene adsorption on various cation-exchanged forms of sepiolite. The novelty of this study is in its comparison of the ethylene adsorption properties of sepiolite samples after both cation exchange and acid activation and in its determination of the most suitable type of sepiolite for optimum adsorption. Hence, the objective of this study is to investigate the possible

*E-mail: burcuerdogan@eskisehir.edu.tr
Cite this article: Erdoğan B, Esenli F (2021). Sepiolite as an efficient adsorbent for ethylene gas. *Clay Minerals* **56**, 222–228. https://doi.org/10.1180/clm.2021.36

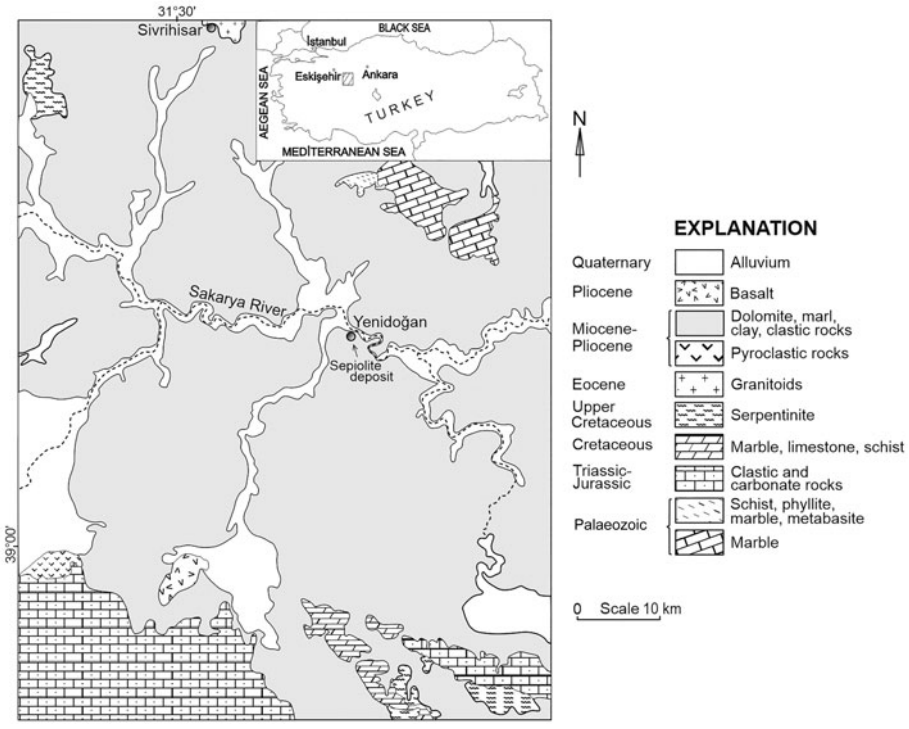

Fig. 1. Geological map of the southern Sivrihisar area and location of the Yenidoğan sepiolite deposit (revised from MTA, 2002; Yeniyol, 2014).

application of this non-toxic, readily available and low-cost material as an adsorbent for removing ethylene and thus extending the shelf-life of vegetables and fruits.

Materials and methods

The clay used as an adsorbent is a natural sepiolite from Sivrihisar, southwest Eskişehir, Turkey, supplied by Element Mineral, Inc. There are two types of sepiolite formations in the Sivrihisar region: the meerschaum type and the layered type. Meerschaum sepiolites have been used for many years in the manufacture of pipes and ornaments due to their ease of cutting and shaping. Such formations occur as fragments of Miocene-aged conglomerates. Layered sepiolites are in Miocene–Pliocene-aged volcaniclastics in the Sivrihisar region. They are economically important mineable deposits and have important applications due to their physicochemical properties.

In the Sivrihisar region, the 200–500 m-thick Miocene–Pliocene volcaniclastic succession unconformably overlies the Palaeozoic metamorphic basement rocks, Mesozoic clastic rocks, carbonates, serpentinites and Eocene granitoids (Fig. 1) (Yeniyol, 1992, 2012; Ece & Çoban, 1994; Karakaş & Varol, 1994; Kadir *et al.*, 2016). The Miocene–Pliocene succession consists of conglomerate, limestone, dolomite, clayey dolomite, sepiolite, gypsum, magnesite and pyroclastics. Three different types of sepiolite beds were recognized in central parts of the Sivrihisar basin: (1) organic matter-rich black sepiolite; (2) organic matter-poor brown sepiolite, which contains ~5% dolomite; and (3) white-, cream- or yellow-coloured dolomitic sepiolite containing 20–40% dolomite (Ece & Çoban, 1994). The layered sepiolite sample with beige–pale brown colour used in this study was obtained from the Yenidoğan area (Fig. 1).

The sepiolite was ground to obtain the <45 μm fraction. Cation-exchanged and acid-activated sepiolites were prepared using $LiNO_3$, KNO_3, $NaNO_3$, $Ca(NO_3)_2$, $Mg(NO_3)_2$, HNO_3 and H_2SO_4 under the following conditions: concentration: 1.0 M; heating temperature: 90°C; reaction time: 4 h; and sample/solution ratio: 5% m/v. The samples were then filtered, washed several times with hot deionized water, dried first at room temperature and then at 100°C for 20 h and kept in a desiccator. The natural sepiolite sample is denoted as S while the Na-S, K-S, Li-S, Mg-S, Ca-S, HN-S and HS-S formulations refer to the samples obtained by cation exchange and acid treatment of the S sample. All of the chemicals were supplied by Merck (Germany).

X-ray diffraction (XRD) analyses were performed using a Bruker (D8 Advance) apparatus with Cu-*Kα* radiation (λ = 1.54 Å) in the 2θ range from 5° to 40° with a 0.02° scanning step. The samples were analysed chemically for major oxides using X-ray fluorescence (XRF) spectroscopy with a Rigaku ZSX Primus XRF spectrometer. The CEC values of the sepiolite samples were determined using the sodium acetate method (Chapman, 1965). Nitrogen adsorption isotherms were measured at 77 K using an Autosorb 1 instrument (Quantachrome, USA). Ethylene adsorption isotherms of the sepiolites were obtained at 273 K using the same instrument. Gas adsorption measurements were made after degassing under vacuum at 125°C for 12 h.

Results and discussion

XRD analysis

The XRD traces of sepiolite and that of the modified forms are displayed in Fig. 2. The sample S consists mainly of sepiolite with minor dolomite (Fig. 2a). A sharp, intense and symmetrical (110) peak at 11.7 Å indicates a relatively well-ordered sepiolite. The full width at half maximum (FWHM) of this peak displays a non-linear relationship with crystallinity. The FWHM of the (110) peak is 0.69°2θ, which is lower than that of the well-ordered sepiolite (Yeniyol, 2014) and higher than that of most of the sepiolites given by Sanchez Del Rio *et al.* (2011).

https://doi.org/10.1180/clm.2021.36 Published online by Cambridge University Press

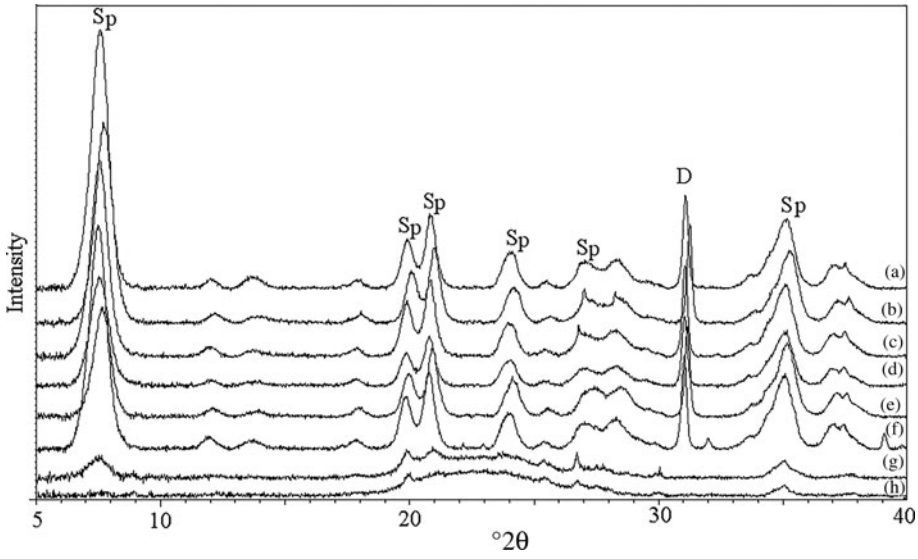

Fig. 2. XRD traces of the (a) raw S, (b) Mg-S, (c) Li-S, (d) Ca-S, (e) K-S, (F) Na-S, (g) HN-S and (h) HS-S samples. D = dolomite; Sp = sepiolite.

The XRD traces of S and the cation-exchanged forms (Na-S, K-S, Li-S, Mg-S and Ca-S) are similar, as expected, indicating that no structural changes occurred during the modification of sepiolite with exchange solutions. The intensity, sharpness and FWHM values of the (110) peak did not differ significantly for the cation-exchanged sepiolites. However, the crystal order was highest in the Mg-exchanged sepiolite and lowest in the Ca-exchanged sepiolite, although the differences were small (Mg > Na > Li > K > Ca). By contrast, the intensities of the main sepiolite peaks of the acid-activated samples significantly decreased due to the partial destruction of the structure (Fig. 2g,h). The decomposition of sepiolite is more pronounced after H_2SO_4 activation than after HNO_3 activation. Sepiolite decomposes faster than palygorskite as its octahedral sheet is richer in Mg^{2+} and its structural micro-channels are larger (Myriam *et al.*, 1998). The disappearance of the dolomite peaks after acid treatment is due to dissolution.

Although the intensities of the sepiolite and dolomite peaks decrease or vanish, there is a broad hump between 20 and 30°2θ on the XRD traces of the acid-activated samples (Fig. 2g,h), which is in accordance with previous works (Myriam *et al.*, 1998; Gonzales-Pradas *et al.*, 2005; Esteban-Cubillo *et al.*, 2008). This hump is related to the presence of the amorphous phase, probably opal-A. Additionally, the presence of sharp but low-intensity peaks on this hump is indicative of quartz and feldspar. These amorphous and crystalline phases were probably present in trace amounts below the XRD detection limit in natural sepiolite (S). They appeared on the XRD traces of the samples shown in Fig. 2g,h after acid treatment due to the partial dissolution of sepiolite and dolomite.

Chemical analysis and CEC

The chemical compositions of the sepiolite samples are listed in Table 1. As the natural sample (S) contains sepiolite and dolomite, the CaO (3.31%) is due to dolomite only and the SiO_2 (52.36%) resides only in sepiolite. Thus, the S sample contains 89% sepiolite and 11% dolomite. However, due to the presence of trace quartz, feldspar and amorphous phases as shown by the XRD results, it may be suggested that the S sample contains ~80% sepiolite.

Portions of the MgO, Al_2O_3, Na_2O, K_2O and Fe_2O_3 come from sepiolite. The Si^{4+} is substituted by Al^{3+} and Fe^{3+} in the tetrahedral sheet, and Al^{3+}, Fe^{3+} and Fe^{2+} are the main cations substituting for Mg^{2+} in the octahedral sheet of the sepiolite structure; therefore, certain amounts of Al_2O_3 and Fe_2O_3 occur in most sepiolites, and other oxides, such as TiO_2, K_2O and Na_2O, are generally present at a very low level or entirely absent (Suarez & Garcia-Romero, 2011). The remaining MgO originates from dolomite. The loss on ignition of the samples is due to the dehydration and dehydroxylation of sepiolite and the decomposition of dolomite (Table 1). The observed changes in chemical compositions considerably varied according to the salt and acid solutions. As a result of acid treatment, the exchangeable cations were removed, the octahedral cations (Mg^{2+}, Al^{3+} and Fe^{3+}) were dissolved and amorphous SiO_2 formed, which is insoluble in the acid solution (Myriam *et al.*, 1998; Gonzalez-Pradas *et al.*, 2005; Lazarevic *et al.*, 2007).

Table 1. Chemical compositions (%) of the natural, cation-exchanged and acid-activated sepiolites.

Sample	SiO_2	Al_2O_3	Fe_2O_3	MgO	CaO	Na_2O	K_2O	LOI
S	52.358	5.786	2.084	19.291	3.306	0.638	0.486	15.882
Na-S	47.637	4.566	1.905	17.094	2.754	4.537	0.442	20.788
K-S	47.969	4.914	1.936	17.680	2.803	0.523	4.997	18.845
Li-S	48.882	5.873	1.915	18.348	2.855	0.299	0.439	21.084
Mg-S	45.539	4.580	1.818	19.434	2.628	0.404	0.419	25.099
Ca-S	42.557	4.550	1.671	16.181	7.627	0.777	0.425	25.778
HN-S	76.961	3.610	1.101	2.104	0.100	0.871	0.577	14.310
HS-S	77.478	3.697	0.539	1.296	0.111	0.840	0.512	14.292

LOI = loss on ignition.

The CEC values of the sepiolite samples are listed in Table 2. The CEC of the raw sepiolite was 23.72 cmol(+) kg^{-1}. This CEC value is within the range 9.5–60.0 cmol(+) kg^{-1} reported in previous studies (Velde, 1992; Brigatti *et al.*, 2000; Alkan *et al.*, 2005; Sun *et al.*, 2014). The CEC values of the acid-activated forms were greater than those of the raw sepiolite and its cation-exchanged forms. The CEC values followed the order Na > natural sepiolite (S) > K > Mg > Li > Ca, although the differences were small. The acid-treated samples showed CEC values which were approximately twice as large, probably because acid treatment removed impurities from the sepiolite channels, especially their external parts.

https://doi.org/10.1180/clm.2021.36 Published online by Cambridge University Press

Table 2. CEC and nitrogen adsorption data of the natural, cation-exchanged and acid-activated sepiolites.

Sample	CEC (cmol(+) kg^{-1})	BET surface area (m^2 g^{-1})	Micropore surface area (m^2 g^{-1})	Micropore volume (10^{-2} cm^3 g^{-1})
S	23.72	248.4	68.8	2.845
Na-S	29.95	192.3	34.9	1.471
K-S	23.24	225.7	62.6	2.631
Li-S	20.53	266.6	81.8	3.434
Mg-S	22.24	234.5	72.4	3.023
Ca-S	17.99	125.2	33.8	1.395
HN-S	53.07	507.9	207.7	11.380
HS-S	50.58	506.9	222.3	9.389

Nitrogen adsorption

The specific surface areas and micropore volumes calculated using the Brunauer–Emmett–Teller (BET) method and *t*-plot method, respectively, are summarized in Table 2. The ion-exchange modification did not increase the specific surface area. The BET surface areas of the Na-, K-, Mg- and Ca-exchanged sepiolite samples are in the range of 125.2–234.5 m^2 g^{-1}, which is lower than that of natural sepiolite (248.4 m^2 g^{-1}). This can be explained by the partial blockage of the channels due to cation exchange, preventing the penetration of N_2 molecules. The treatment with 1.0 M HNO_3 and H_2SO_4 solutions increased considerably the specific surface area (from 248.4 m^2 g^{-1} for S to 507.9 m^2 g^{-1} for HN-S and 506.9 m^2 g^{-1} for HS-S), the micropore surface area (from 68.8 m^2 g^{-1} for S to 207.7 m^2 g^{-1} for HN-S and 222.3 m^2 g^{-1} for HS-S) and the micropore volume (from 2.845×10^{-2} cm^3 g^{-1} for S to 11.380×10^{-2} cm^3 g^{-1} for HN-S and to 9.389×10^{-2} cm^3 g^{-1} for HS-S) (Table 2), which is in accordance with previous work (Myriam *et al.*, 1998; Dekany *et al.*, 1999; Gonzales-Pradas *et al.*, 2005; Lazarevic *et al.*, 2007). The increase in the specific surface area may be explained by the dissolution of the brucite layer, the elimination of soluble impurities and the increase in the number of the micropores.

Adsorption of ethylene

The ethylene adsorption isotherms obtained at 273 K and up to 100 kPa are shown in Figs 3 & 4. As the kinetic diameter of the ethylene molecule is 3.9 Å, it can easily enter into the channels

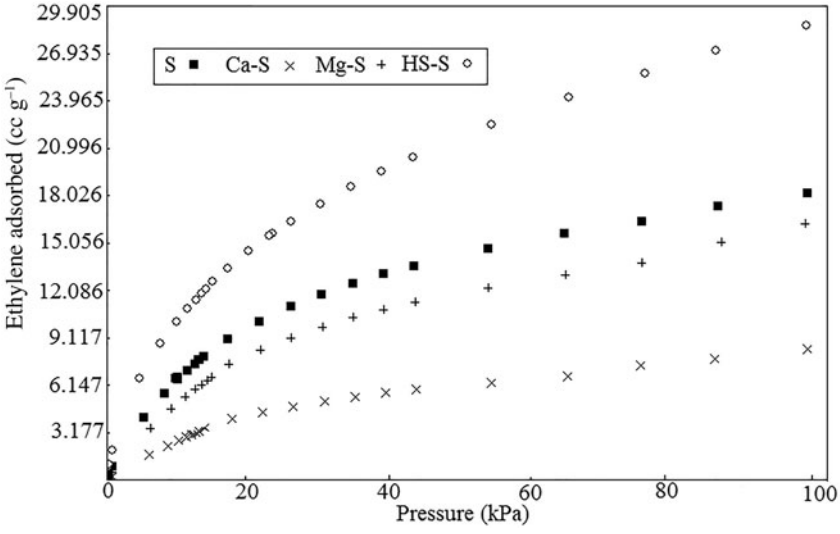

Fig. 3. Ethylene adsorption isotherms of the S, Ca-S, Mg-S and HS-S samples at 273 K.

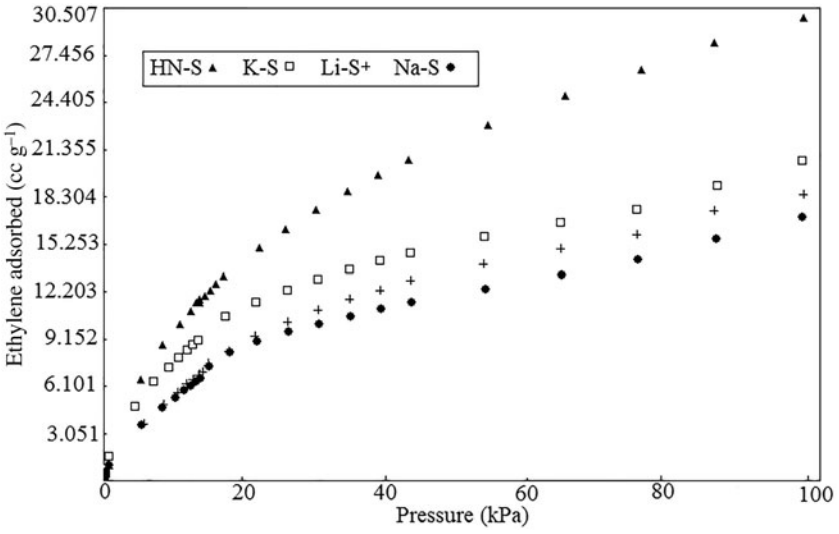

Fig. 4. Ethylene adsorption isotherms of the HN-S, K-S, Li-S and Na-S samples at 273 K.

https://doi.org/10.1180/clm.2021.36 Published online by Cambridge University Press

Table 3. Comparison of the ethylene adsorption capacities of the present work with literature data.

Sample	Temperature (K)	Pressure (kPa)	Adsorption capacity (mmol g^{-1})	Reference
PILC-6	273	100	0.570	Youngjan (2012)
PCHA	273	100	1.436	Youngjan (2012)
Olesorb-1	303	100	1.17	Choundry *et al.* (2002)
PILC	273/318	733	1.49/ 0.81	Saini *et al.* (2011)
PCH1	298/318	750	2.32/1.29	Saini *et al.* (2011)
PCH2	298/318	754	2.37/1.85	Saini *et al.* (2011)
SH	273/293	37	0.859/0.572	Erdoğan Alver & Sakızcı (2012)
K1H	273/293	37	0.046/0.021	Erdoğan Alver & Sakızcı (2012)
K2H	273/293	37	0.061/0.027	Erdoğan Alver & Sakızcı (2012)
B1H	273/293	37	0.121/0.091	Erdoğan Alver & Sakızcı (2012)
B2H	273/293	37	0.144/0.136	Erdoğan Alver & Sakızcı (2012)
BH3-5	273	100	0.627	Erdoğan Alver *et al.* (2016)
BH6-5	273	100	0.719	Erdoğan Alver *et al.* (2016)
B	273	100	0.292	Erdoğan Alver (2017)
Ag-B	273	100	1.817	Erdoğan Alver (2017)
K-B	273	100	0.335	Erdoğan Alver (2017)
Li-B	273	100	0.240	Erdoğan Alver (2017)
Mg-B	273	100	0.201	Erdoğan Alver (2017)
Cu-B	273	100	0.239	Erdoğan Alver & Günal (2016)
Fe-B	273	100	0.167	Erdoğan Alver & Günal (2016)
S	273	100	0.813	Present study
Na-S	273	100	0.749	Present study
K-S	273	100	0.907	Present study
Li-S	273	100	0.812	Present study
Mg-S	273	100	0.727	Present study
Ca-S	273	100	0.376	Present study
HN-S	273	100	1.308	Present study
HS-S	273	100	1.279	Present study

of sepiolite. The ethylene adsorption capacities of sepiolite and those of modified forms were compared with those reported in the literature (Table 3). In samples prepared using cation exchange, ethylene adsorption capacities are comparable, and the order of these capacities is K-S > Li-S > Na-S > Mg-S > Ca-S. Although the specific surface area of the K-S sample was moderate (225.7 m^2 g^{-1}), it displayed the greatest adsorption selectivity due to the stronger cation–π interactions of K^+ with ethylene molecules than the Na^+, Mg^{2+}, Li^+ and Ca^{2+} cations. The C_2H_4 adsorption capacity of Li-S (0.812 mmol g^{-1}) was greater than those of Na-S (0.749 mmol g^{-1}), Mg-S (0.727 mmol g^{-1}) and Ca-S (0.376 mmol g^{-1}). For sepiolite exchanged with large cations such as Na^+ and Ca^{2+}, the contribution of cation–π interactions is considerable, the large ions may also block the adsorption sites and reduce the ethylene adsorption capacity. The lowest affinity of Ca-S for ethylene may be ascribed to both its lowest specific surface area and the blockages of the adsorption sites, which arise from large populations of large Ca^{2+} ions on the sepiolite surface.

The HN-S and HS-S samples were better adsorbents for the retention of C_2H_4 compared to the cation-exchanged forms (Table 3). This was probably due to an increase in the cross-section of the intercrystalline channels caused by the exchange of large cations, such as K^+, Na^+ and Ca^{2+}, with small H^+ cations, as well as being due to the obvious increase in the microporosity and specific surface area of sepiolite, leading to an increase in the rate of diffusion of ethylene molecules into the channels of sepiolite. In addition, the dissolution of octahedral cations (e.g. Mg^{2+}) as a result of the acid treatment yielded fresh silanol groups. Due to their double bonds, high polarizability and quadrupole moment, ethylene molecules interact with the surface of HN-S more strongly than with the other modified forms. The HN-S sample had a greater ethylene adsorption capacity than pillared bentonite (PILC-6; 0.570 mmol g^{-1} at 273 K) (Youngjan, 2012), bentonite (0.292 mmol g^{-1}) and its K^+-exchanged (0.335 mmol g^{-1}), Li^+-exchanged (0.240 mmol g^{-1}), Mg^{2+}-exchanged (0.201 mmol g^{-1}) forms (Erdoğan Alver, 2017), Cu^{2+}-exchanged (0.239 mmol g^{-1}) and Fe^{3+}-exchanged (0.167 mmol g^{-1}) bentonites at 273 K (Erdoğan Alver & Günal, 2016) and bentonite treated with 5.0 M HCl for 3 and 6 h (BH3-5 = 0.627 and BH6-5 = 0.719 mmol g^{-1}) (Erdoğan Alver *et al.*, 2016) (Table 3). This can be explained by the presence of channels in the sepiolite structure, unlike in bentonite. The gas adsorption characteristics of the clay minerals are largely dependent on the porosity, the specific surface area and the active sorption sites (especially silanol groups) of the adsorbent and the polarity and size of the adsorbate molecules (Galán, 1996). By contrast, bentonite treated with 4.8 mL solution of 0.5 M cetyltrimethylammonium bromide solution displayed a greater capacity for the adsorption of ethylene than the HN-S sample due to its textural and structural differences (1.436 mmol g^{-1}) (Youngjan, 2012). All of these samples are different from the sample in the present study and different conditions were implemented during treatment. In conclusion, the sepiolite treated with 1.0 M HNO_3 solution is the most effective adsorbent (1.308 mmol g^{-1}) for the removal of ethylene from storage environments.

Summary and conclusions

The C_2H_4 adsorption experiments with the sepiolite sample from the Sivrihisar region, Turkey, were carried out to determine the usability of this low-cost mineral and that of the cation-exchanged (Na-S, K-S, Li-S, Mg-S and Ca-S) and acid-activated (HN-S and HS-S) forms for the removal of ethylene. The acid treatment caused significant structural changes to sepiolite. The acid-treated forms of sepiolite are more effective for the adsorption of ethylene than the cation-exchanged forms. This can be attributed to the

https://doi.org/10.1180/clm.2021.36 Published online by Cambridge University Press

blocking of the channels of sepiolite as a result of the cation exchange, which prevents ethylene adsorption. Among the sepiolite samples studied, the maximum ethylene adsorption capacity was determined for sepiolite activated with 1.0 M HNO_3 solution (HN-S). In summary, HN-S can be used as an efficient and low-cost adsorbent to control ethylene in storage environments, and therefore it may extend the shelf-life of fruits and vegetables.

References

Alkan M., Çelikçapa S., Demirbaş Ö. & Doğan M. (2005) Removal of reactive blue 221 and acid blue 62 anionic dyes from aqueous solutions by sepiolite. *Dyes and Pigments*, **65**, 251–259.

Alvarez-Hernandez M., Artes-Hernandez, F., Avalos-Belmontes F., Castillo-Campohermoso M.A., Contreras-Esquivel J.C., Ventura-Sobrevilla J.M. & Martinez-Hernandez G.B. (2018) Current scenario of adsorbent materials used in ethylene scavenging systems to extend fruit and vegetable postharvest life. *Food and Bioprocess Technology*, **11**, 511–525.

Brigatti M.F., Galán E. & Theng, B.K.G. (2006) Structures and mineralogy of clay minerals. Pp. 21–81 in: *Handbook of Clay Science* (F. Bergaya, B.K.G. Theng & G. Lagaly, editors). Elsevier, Amsterdam, The Netherlands.

Brigatti M.F., Lugli C. & Poppi L. (2000) Kinetics of heavy-metal removal and recovery in sepiolite. *Applied Clay Science*, **16**, 45–57.

Chapman H.D. (1965) Cation exchange capacity. Pp. 891–901 in: *Methods of Soil Analysis* (C.A. Black, editor). American Society of Agronomy, Madison, WI, USA.

Cho S.H., Park J.H., Han S.S. & Kim J.N. (2005) Comparison of $AgNO_3$/clay and $AgNO_3$/ALSG sorbent for ethylene separation. *Adsorption*, **11**, 145–149.

Choundary N.V., Kumar P., Bhat T.S.G., Cho S.H., Han S.S. & Kim J.N. (2002) Adsorption of light hydrocarbon gases on alkene-selective adsorbent. *Industrial & Engineering Chemistry Research*, **41**, 2728–2734.

Dekany I., Turi L., Fonseca A. & Nagy J.B. (1999) The structure of acid treated sepiolites: small-angle X-ray scattering and multi MAS-NMR investigations. *Applied Clay Science*, **14**, 141–160.

Ece Ö.I. & Çoban F. (1994) Geology, occurrence, and genesis of Eskisehir sepiolites, Turkey. *Clays and Clay Minerals*, **42**, 81–92.

Erdoğan Alver B. (2017) Adsorption studies of hydrogen and ethylene on cation-exchanged bentonite. *Clay Minerals*, **52**, 67–73.

Erdoğan Alver B. & Günal A. (2016) Thermal, structural and ethylene adsorption properties of Ag-, Cu- and Fe-modified bentonite from Turkey. *Journal of Thermal Analysis Calorimetry*, **126**, 1533–1540.

Erdoğan Alver B. & Sakızcı M. (2012) Ethylene adsorption on acid-treated clay minerals. *Adsorption Science & Technology*, **30**, 265–273.

Erdoğan Alver B., Alver Ö., Günal A. & Dikmen G. (2016) Effects of hydrochloric acid treatment on structure characteristics and C_2H_4 adsorption capacities of Ünye bentonite from Turkey: a combined FT-IR, XRD, XRF, TG/DTA and MAS NMR study. *Adsorption*, **22**, 287–296.

Esteban-Cubillo A., Pina-Zapardiel R., Moya J.S., Barba M.F. & Pecharroman C. (2008) The role of magnesium on the stability of crystalline sepiolite structure. *Journal of the European Ceramic Society*, **28**, 1763–1768.

Gaikwad K.K., Singh S. & Negi Y.S. (2019) Ethylene scavengers for active packaging of fresh food produce. *Environmental Chemistry Letters*, **18**, 1–16.

Galán E. (1996) Properties and applications of palygorskite–sepiolite clays. *Clay Minerals*, **31**, 443–453.

Gonzalez-Pradas E., Socias-Viciana M., Urena-Amate M.D., Cantos-Molina A. & Villafranca-Sanchez M. (2005) Adsorption of chloridazon from aqueous solution on heat and acid treated sepiolites. *Water Research*, **39**, 1849–1857.

Gwak G.H., Kim H.J., Oh J.M., Lee S.W., Kwon Y.C. & Han Y.S. (2017) Ethylene scavenging ability of permanganate incorporated nanoclays. *Journal of Nanoscience and Nanotechnology*, **17**, 3576–3580.

Iqbal N., Khan N.A., Ferrante A., Trivellini A., Francini A. & Khan M.I.R. (2017) Ethylene role in plant growth, development and senescence: interaction with other phytohormones. *Frontiers in Plant Science*, **8**, 1–19.

Jones B.F. & Galán, E. (1988) Sepiolite and palygorskite. Pp. 631–674 in: *Hydrous Phyllosilicates* (S.W. Bailey, editor). Mineralogical Society of America, Washington, DC, USA.

Kadir S., Erkoyun H., Eren M., Huggett J. & Önalgil N. (2016) Mineralogy, geochemistry, and genesis of sepiolite and palygorskite in Neogene lacustrine sediments, Eskişehir Province, west central Anatolia, Turkey. *Clays and Clay Minerals*, **64**, 145–166.

Karakaş Z. & Varol B. (1994) Petrography of lacustrine dolomites in Sivrihisar Neogene basin and interpretation of their depositional environment using stable isotopes ($d^{18}O$; $d^{13}C$). *Mineral Research and Exploration Bulletin of Turkey*, **116**, 23–38.

Komadel P. (2003) Chemically modified smectites. *Clay Minerals*, **38**, 127–138.

Komadel P. & Madejová J. (2006) Acid activation of clay minerals. Pp. 263–287 in: *Handbook of Clay Science* (F. Bergaya, B.K.G. Theng & G. Lagaly, editors). Elsevier, Amsterdam, The Netherlands.

Lazarevic S., Jankovic-Castvan, I., Jovanovic. D., Milonjic S., Janackovic D. & Petrovic R. (2007) Adsorption of Pb^{2+}, Cd^{2+} and Sr^{2+} ions onto natural and acid-activated sepiolites. *Applied Clay Science*, **37**, 47–57.

Lee J.W., Park J.H., Han S.S., Kim J.N., Cho S.H. & Lee, Y.T. (2005) Adsorption equilibrium and dynamics of C_4 olefin/paraffin on π-complexing adsorbent. *Separation Science and Technology*, **39**, 1365–1384.

MTA (2002) *1:500,000 Scale Geological Map Series of Turkey, Ankara Sheet*. General Directorate of Mineral Research and Exploration, Ankara, Turkey. Available from https://www.mta.gov.tr/en/maps/geological-500000

Murray H.H. (2007) *Applied Clay Mineralogy: Occurrences, Processing, and Application of Kaolins, Bentonites, Palygorskite–Sepiolite, and Common Clays*. Elsevier, Amsterdam, The Netherlands, 188 pp.

Myriam M., Suarez M. & Martin-Pozas J.M. (1998) Structural and textural modifications of palygorskite and sepiolite under acid treatment. *Clays and Clay Minerals*, **46**, 225–231.

Park J.H., Han S.S., Kim J.N. & Cho S.H. (2004) Vacuum swing adsorption process for the separation of ethylene/ethane with $AgNO_3$/clay adsorbent. *Korean Journal of Chemical Engineering*, **21**, 236–245.

Park J.H., Lee H.K., Han S.S., Kim J.N. & Cho S.H. (2002) Adsorption equilibrium of ethane/ethylene on $AgNO_3$/clay adsorbent. *Korean Chemical Engineering Research*, **40**, 467–473.

Reid M.S. (1995) Ethylene in plant growth, development, and senescence. Pp. 486–508 in: *Plant Hormones* (P.J. Davis, editor). Springer, Dordrecht, The Netherlands.

Rodriguez-Reinoso F., Ramirez-Saenz A., Lopez-Gonzalez J.D.D., Valenzuela-Calahorro C. & Zurita-Herrera L. (1981) Activation of a sepiolite with dilute solutions of HNO_3 and subsequent heat treatments: III. Development of porosity. *Clay Minerals*, **16**, 315–323.

Saini V.K., Pinto M. & Pires J. (2011) High pressure adsorption studies of ethane and ethylene on clay based adsorbent materials. *Separation Science Technology*, **46**, 137–146.

Sanchez Del Rio, M., García-Romero E., Suarez M., Da Silva I., Fuentes-Montero L. & Martínez-Criado G. (2011) Variability in sepiolite: diffraction studies. *American Mineralogist*, **96**, 1443–1454.

Srithammaraj K., Magaraphan R. & Manuspiya H. (2018) Influence of thiol groups on the ethylene adsorption and conductivity properties of the modified porous clay heterostructures (PCHS) using as ethylene scavenger in smart packaging. *Polymer Bulletin*, **75**, 3951–3969.

Suarez M. & Garcia-Romero E. (2011) Advances in the crystal chemistry of sepiolite and palygorskite. Pp. 33–65 in: *Developments in Clay Science, Vol. 3* (E. Galán & A. Singer, editors). Elsevier, Amsterdam, The Netherlands.

Sun Y., Li J. & Wang X. (2014) The retention of uranium and europium onto sepiolite investigated by macroscopic, spectroscopic and modeling techniques. *Geochimica et Cosmochimica Acta*, **140**, 621–643.

Velde B. (1992) *Introduction to Clay Minerals*. Chapman & Hall, London, UK, 198 pp.

Vicente Rodriguez M.A., Lopez Gonzalez J.D.D. & Banares Munoz M.A. (1994) Acid activation of a Spanish sepiolite: physicochemical characterization, free silica content and surface area of products obtained. *Clay Minerals*, **29**, 361–367.

https://doi.org/10.1180/clm.2021.36 Published online by Cambridge University Press

Yeniyol M. (1992) Geology, mineralogy and genesis of Yenidoğan (Sivrihisar) sepiolite deposit. *Mineral Research and Exploration Bulletin of Turkey*, **114**, 51–64.

Yeniyol M. (2012) Geology and mineralogy of a sepiolite–palygorskite occurrence from SW Eskisehir (Turkey). *Clay Minerals*, **47**, 93–104.

Yeniyol M. (2014). Characterization of two forms of sepiolite and related Mg-rich clay minerals from Yenidoğan (Sivrihisar, Turkey). *Clay Minerals*, **49**, 91–108.

Youngjan S. (2012) *Ethylene Adsorption on Modified Bentonite*. Master's thesis, Department of Chemistry, Suranaree University of Technology, Thailand, 97 pp.

https://doi.org/10.1180/clm.2021.36 Published online by Cambridge University Press